



Cite this: *Nanoscale*, 2015, 7, 13547

## Enhanced second harmonic generation of MoS<sub>2</sub> layers on a thin gold film†

Jianhua Zeng,<sup>a</sup> Maohui Yuan,<sup>a</sup> Weiguang Yuan,<sup>a</sup> Qiaofeng Dai,<sup>a</sup> Haihua Fan,<sup>a</sup> Sheng Lan\*<sup>a</sup> and Shaolong Tie\*<sup>b</sup>

The linear and nonlinear optical properties of thin MoS<sub>2</sub> layers exfoliated on an Au/SiO<sub>2</sub> substrate were investigated both numerically and experimentally. It was found that the MoS<sub>2</sub> layers with different thicknesses exhibited different colors on the gold film. The reflection spectra of the MoS<sub>2</sub> layers with different thicknesses were calculated by using the finite-difference time-domain technique and the corresponding chromaticity coordinates were derived. The electric field enhancement factors at both the fundamental light and the second harmonic were calculated and the enhancement factors for second harmonic generation (SHG) were estimated for the MoS<sub>2</sub> layers with different thicknesses. Different from the MoS<sub>2</sub> layers on a SiO<sub>2</sub>/Si substrate where the maximum SHG was observed in the single-layer MoS<sub>2</sub>, the maximum SHG was achieved in the 17 nm-thick MoS<sub>2</sub> layer on the Au/SiO<sub>2</sub> substrate. As compared with the MoS<sub>2</sub> layers on the SiO<sub>2</sub>/Si substrate, a significant enhancement in SHG was found for the MoS<sub>2</sub> layers on the Au/SiO<sub>2</sub> substrate due to the strong localization of the electric field. More interestingly, it was demonstrated experimentally that optical data storage can be realized by modifying the SHG intensity of a MoS<sub>2</sub> layer through thinning its thickness.

Received 13th May 2015,  
Accepted 30th June 2015

DOI: 10.1039/c5nr03133h

www.rsc.org/nanoscale

## 1 Introduction

In recent years, two-dimensional (2D) materials have attracted tremendous interest owing to their fascinating and technologically useful properties.<sup>1,2</sup> Apart from graphene, much attention has been paid to transition metal dichalcogenides (TMDs) because they exhibit many properties different from graphene,<sup>3–9</sup> and MoS<sub>2</sub> is the most intensively and extensively studied TMD.<sup>10–18</sup> So far, the physical properties of MoS<sub>2</sub>, especially the mechanical, electronic and optical properties, have been deeply investigated and their potential applications in logic electronics,<sup>19,20</sup> integrated circuits,<sup>21,22</sup> flexible electronics,<sup>23–25</sup> optoelectronics and photonics have been explored.<sup>26–28</sup> Recently, the nonlinear optical responses of MoS<sub>2</sub> have become the focus of many studies because they play an important role in the photonic applications in which ultrafast laser pulses with high peak powers are generally used. Although a bulk MoS<sub>2</sub> crystal with 2H stacking order is expected to have vanished second-order nonlinear suscepti-

bility ( $\chi^{(2)}$ ) because of the inversion symmetry,<sup>29</sup> it has been demonstrated that MoS<sub>2</sub> with odd layers, especially the single-layer one, exhibits efficient second harmonic generation (SHG) arising from the breaking of the inversion symmetry.

Very recently, much effort has been devoted to the study of SHG in MoS<sub>2</sub>. In 2013, several research groups reported independently the observation of highly efficient SHG from single-layer MoS<sub>2</sub>, the dependence of the SHG intensity on the number of layers of MoS<sub>2</sub> and the polarization of the excitation laser, and the applications of SHG spectroscopy in determining the crystalline orientation, thickness uniformity, layer stacking and single-crystal domain.<sup>30–32</sup> Kumar *et al.* derived a second-order nonlinear susceptibility  $\chi^{(2)}$  on the order of  $\sim 10^{-7}$  m V<sup>-1</sup> for single-layer MoS<sub>2</sub>. They also found a reduction of SHG by a factor of seven in trilayered MoS<sub>2</sub> and by two orders of magnitude in MoS<sub>2</sub> with even layers.<sup>30</sup> Large second-order nonlinear susceptibility with a similar value was also observed by Malard *et al.*<sup>31</sup> Li *et al.* measured and compared the SHG in thin MoS<sub>2</sub> and h-BN with one to five layers and also observed strong SHG from materials with odd layers and no appreciable SHG from materials with even layers.<sup>32</sup> More interestingly, Hsu *et al.* investigated the SHG from homo- and heterostructural TMD bilayers formed by artificial stacking with an arbitrary angle.<sup>33</sup> They found that the SHG from the twisted bilayers is a coherent superposition of the SH fields from the individual layers, with a phase difference depending on the stacking angle. Yin *et al.* reported the observation of an

<sup>a</sup>Guangdong Provincial Key Laboratory of Nanophotonic Functional Materials and Devices, School of Information and Optoelectronic Science and Engineering, South China Normal University, Guangzhou 510006, P. R. China. E-mail: slan@sncu.edu.cn

<sup>b</sup>School of Chemistry and Environment, South China Normal University, Guangzhou 510006, P. R. China. E-mail: tiesl@sncu.edu.cn

†Electronic supplementary information (ESI) available. See DOI: 10.1039/c5nr03133h

enhancement in SHG at the edges of the MoS<sub>2</sub> layer.<sup>34</sup> Wang *et al.* observed a third harmonic generation in thin MoS<sub>2</sub> layers and deduced a third-order nonlinear susceptibility which is comparable to the commonly used semiconductors under resonant conditions.<sup>35</sup>

So far, the substrates commonly used for studying MoS<sub>2</sub> are SiO<sub>2</sub>/Si substrates because atomically thin MoS<sub>2</sub> layers on a SiO<sub>2</sub>/Si substrate exhibit different colors which depend strongly on the thicknesses of the MoS<sub>2</sub> layers. Since the color of a thin MoS<sub>2</sub> layer is governed by the reflection spectrum of the combined structure (*i.e.*, MoS<sub>2</sub> + substrate), the substrate plays a crucial role in determining the color of the MoS<sub>2</sub> layer placed on it. This feature makes it easy to identify MoS<sub>2</sub> with few layers. Similar to the influence of the substrate on the reflection spectrum of a MoS<sub>2</sub> layer which exhibits linear optical properties, the existence of the substrate may modify significantly the nonlinear optical responses of the MoS<sub>2</sub> layer, especially in the case when a thin metal film is used just beneath the MoS<sub>2</sub> layer.

In this paper, we investigated the SHG of thin MoS<sub>2</sub> layers on a 50 nm-thick gold film deposited on a silica substrate. It was found that the nonlinear optical responses of MoS<sub>2</sub> layers were modified significantly and the maximum SHG was achieved in a MoS<sub>2</sub> layer with a thickness of ~17 nm, in sharp contrast to the MoS<sub>2</sub> layers on SiO<sub>2</sub>/Si substrates. Based on the numerical simulations by using the finite-difference time-domain (FDTD) technique, it was revealed that the large enhancement in SHG originated mainly from the strongly localized electric field in the MoS<sub>2</sub> layers induced by the thin gold film. As one of the potential applications, this unique thickness dependence of the SHG intensity was exploited to realize optical data storage through thinning the MoS<sub>2</sub> layers.

## 2 Experimental section

MoS<sub>2</sub> layers with different thicknesses were exfoliated on a SiO<sub>2</sub>/Si substrate and an Au/SiO<sub>2</sub> substrate. The latter was formed by depositing a 50 nm-thick gold film on a silica substrate of ~360 μm. The colors exhibited by the MoS<sub>2</sub> layers were examined under a microscope. The Raman spectra of the MoS<sub>2</sub> layers were recorded by using a Raman spectrometer (Invia, Renishaw) at excitation wavelengths of 785 nm and 514 nm. An 800 nm femtosecond (fs) laser light with a repetition rate of 76 MHz and a duration of 130 fs delivered by a fs oscillator (Mira 900S, Coherent) was focused on the MoS<sub>2</sub> layers by using the 60× objective lens (NA = 0.85) of an inverted microscope (Axio Observer A1, Zeiss). The nonlinear optical signals generated by the MoS<sub>2</sub> layers were obtained by using the same objective lens and directed to a combination of a spectrometer (SR-500i-B1, Andor) and a coupled-charge device (DU970N, Andor) for analysis (see ESI, Fig. S1†). For optical data storage, the sample was placed on a three-dimensional positioning system (P-563.3CD, Physik Instruments) with an accuracy of 1 nm for all dimensions. The laser power used

for data recording was much larger than that used for data readout.

For the calculation of the reflection spectra of the MoS<sub>2</sub> layers and the electric field distributions inside the MoS<sub>2</sub> layers, the FDTD technique was employed.<sup>36</sup> The chromaticity coordinates for the MoS<sub>2</sub> layers were derived from the reflection spectra based on the theory of colorimetry. For numerical simulation, the wavelength dependent complex refractive indexes for single-layer and bulk MoS<sub>2</sub> were chosen to be the values that are commonly used.<sup>37,38</sup> For calculation of the electric field enhancement factors, a continuous wave was employed to approximate the pulse train used in the experiments. A nonuniform grid as well as a perfectly matched boundary condition was employed for the numerical simulation.

## 3 Results and discussion

### 3.1 Colors exhibited by the MoS<sub>2</sub> layers with different thicknesses on the Au/SiO<sub>2</sub> substrate

The MoS<sub>2</sub> layers exfoliated on the Au/SiO<sub>2</sub> substrate exhibit different colors, as shown in Fig. 1(A) where one can see some typical colors such as pale violet red (a), medium orchid (b), medium blue (c), deep sky blue (d), pale turquoise (e), light blue (f), medium purple (g), and thistle (h). The colors exhibited by the MoS<sub>2</sub> layers depend strongly on their thicknesses (*d*). In general, Raman scattering spectroscopy is employed to determine the number of atomic layers of the few-layer MoS<sub>2</sub> on SiO<sub>2</sub>/Si substrates.<sup>39</sup> It relies on the fact that the frequency difference between the E<sub>2g</sub><sup>1</sup> and A<sub>1g</sub> vibration modes is closely related to the number of atomic layers. However, this method is not applicable for MoS<sub>2</sub> with atomic layers larger than five because the frequency difference between the two vibration modes remains almost unchanged. Another way to directly determine the thicknesses of MoS<sub>2</sub> layers relies on atomic force microscopy measurements. Previously, it has been shown that a highly absorptive thin film placed on a highly reflective substrate can exhibit different colors that depend strongly on the thickness of the film.<sup>40–42</sup> In this case, one can easily calculate the reflection spectrum of the thin film with a certain thickness and deduce the chromaticity coordinates of the thin film. By correlating the calculated chromaticity coordinate with the actually observed color, one can give a rough estimation of the thickness of the thin film.

In order to calculate the reflection spectra of the MoS<sub>2</sub> layers on the Au/SiO<sub>2</sub> substrate, we need to know the complex refractive indexes of the MoS<sub>2</sub> layers. Basically, the complex refractive indexes for single-layer and bulk MoS<sub>2</sub> are different because the former is a direct semiconductor while the latter is an indirect one (see ESI Fig. S2†). However, it is confirmed that the difference in the complex refractive index has a negligible influence on the calculated reflection spectra (see ESI Fig. S3†). By using FDTD simulation, we have calculated the reflection spectra for MoS<sub>2</sub> layers with different thicknesses, as shown in Fig. 1(B). It can be seen that the reflection spectra

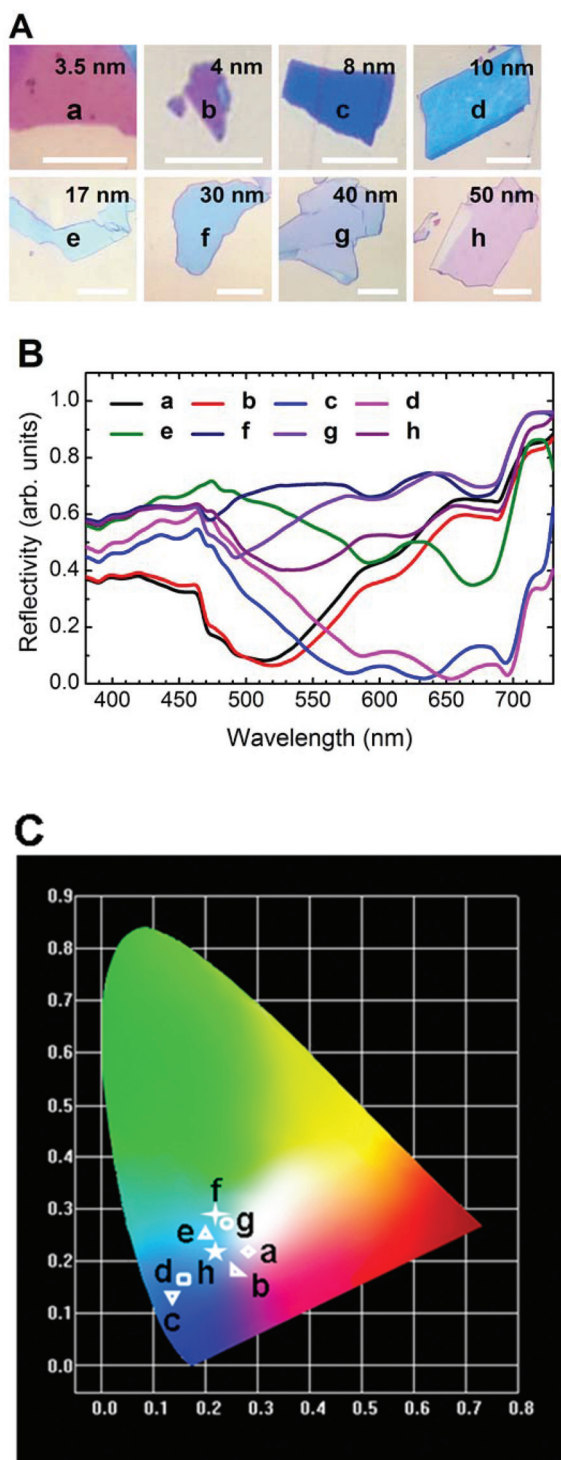


**Fig. 1** (A) Colors exhibited by the MoS<sub>2</sub> layers with different thicknesses on the Au/SiO<sub>2</sub> substrate. a:  $d \approx 3.5$  nm, b:  $d \approx 4.0$  nm, c:  $d \approx 8.0$  nm, d:  $d \approx 10.0$  nm, e:  $d \approx 17$  nm, f:  $d \approx 30$  nm, g:  $d \approx 40$  nm, h:  $d \approx 50$  nm. In each case, the length of the scale bar is 10  $\mu\text{m}$ . (B) Calculated reflection spectra for the MoS<sub>2</sub> layers with different thicknesses on the Au/SiO<sub>2</sub> substrate. (C) Chromaticity coordinates calculated for the MoS<sub>2</sub> layers with different thicknesses on the Au/SiO<sub>2</sub> substrate based on the reflection spectra shown in (B).

appear to be much different when the thickness of the MoS<sub>2</sub> layer is varied. Based on the theory of colorimetry, one can easily deduce the chromaticity coordinates for the MoS<sub>2</sub> layers based on the reflection spectra, as shown in Fig. 1(C). By comparing the chromaticity coordinates and the observed colors, one can give a rough estimation of the thicknesses of the MoS<sub>2</sub> layers, as indicated in Fig. 1(A). It is apparent that the colors exhibited by the MoS<sub>2</sub> on the Au/SiO<sub>2</sub> substrate are more abundant than those observed for the MoS<sub>2</sub> layers on the SiO<sub>2</sub>/Si substrate. The reason is that the highly reflective substrate makes the reflection spectrum of a MoS<sub>2</sub> layer change sensitively with its thickness, even for thick MoS<sub>2</sub> layers.

We measured the Raman scattering spectra for the MoS<sub>2</sub> layers with different thicknesses in which one can easily identify three modes denoted as E<sub>2g</sub><sup>1</sup>, A<sub>1g</sub>, and 2LA(M), corresponding to the in-plane vibration mode, the out-of-plane vibration mode and the double longitudinal acoustic phonon mode (at M point), respectively (see ESI Fig. S5†). The frequency difference between the E<sub>2g</sub><sup>1</sup> and A<sub>1g</sub> modes is 25.3 cm<sup>-1</sup> while that between the A<sub>1g</sub> and 2LA(M) modes is 44.6 cm<sup>-1</sup>. In our case, no obvious difference in the frequency difference between the E<sub>2g</sub><sup>1</sup> and A<sub>1g</sub> modes is found between the thin and thick MoS<sub>2</sub> layers because the number of atomic layers in the thinnest MoS<sub>2</sub> layer ( $d \approx 3.5$  nm) is larger than five.

### 3.2 Second harmonic generation from the MoS<sub>2</sub> layers on the Au/SiO<sub>2</sub> substrate

The nonlinear optical responses of the MoS<sub>2</sub> layers on the Au/SiO<sub>2</sub> substrate were characterized by using a fs laser light at 800 nm and compared with the MoS<sub>2</sub> layers on the SiO<sub>2</sub>/Si substrate. For the MoS<sub>2</sub> layers on the SiO<sub>2</sub>/Si substrate, strong SHG was observed only for the single-layer MoS<sub>2</sub>, similar to the results reported previously.<sup>30–34</sup> For the bulk MoS<sub>2</sub>, the SHG intensity was reduced significantly because of inversion symmetry. In contrast, a significant enhancement in SHG was found for the bulk MoS<sub>2</sub> on the Au/SiO<sub>2</sub> substrate. More interestingly, the thickness dependence of the SHG intensity also changed. In Fig. 2(A), we present the evolution of the nonlinear response spectrum with increasing excitation power measured for the MoS<sub>2</sub> layer with  $d \approx 8$  nm. The fitting of the experimental data for the dependence of the SHG intensity on the excitation power plotted in a double logarithmic coordinate gives a slope of 2.07, which is in good agreement with the second-order nature of the SHG. Under the same conditions, we measured the evolution of the nonlinear response spectrum with increasing excitation power for the MoS<sub>2</sub> layer with  $d \approx 17$  nm and extracted the dependence of the SHG intensity on the excitation power, as shown in Fig. 2(B). In this case, the SHG intensity is almost one order of magnitude larger than that observed for the MoS<sub>2</sub> layer with  $d \approx 8$  nm for excitation powers smaller than 30 mW. For excitation powers larger than 30 mW, the SHG intensity is still six times larger. In the excitation power dependent SHG intensity, a slope of  $\sim 2.04$  is observed at low excitation powers. It is reduced to  $\sim 1.57$  at high excitation powers because of the ablation of the MoS<sub>2</sub> layer by the fs laser light.

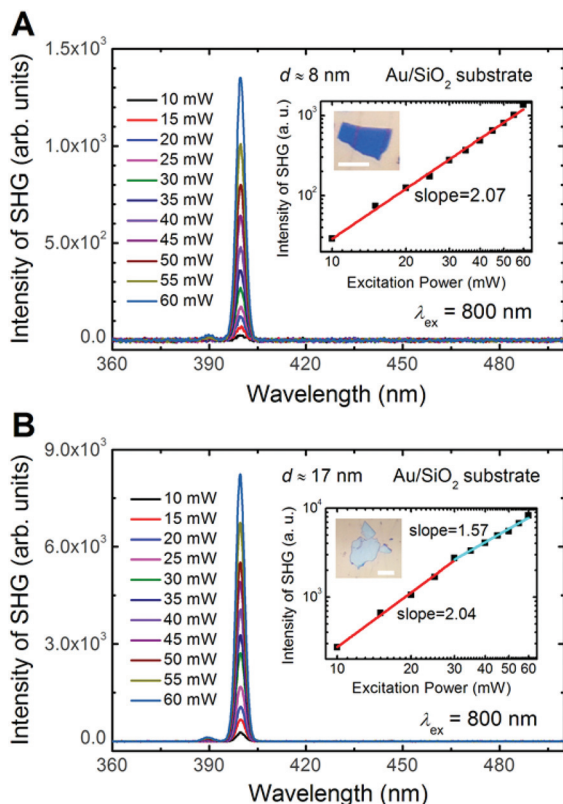


**Fig. 2** Nonlinear response spectra measured for the MoS<sub>2</sub> layers on the Au/SiO<sub>2</sub> substrate with  $d \approx 8$  nm (A) and  $d \approx 17$  nm (B). The insets show the dependence of the SHG intensity on the excitation power plotted in a double logarithmic coordinate and the fitting of the experimental data. The images of the samples are also provided and the length of the scale bar is 10  $\mu\text{m}$ .

Since a strong localization of the electric field is expected to appear in the MoS<sub>2</sub> layers on the Au/SiO<sub>2</sub> substrate, this behavior indicates that the SHG in the MoS<sub>2</sub> layers is no longer dominated by inversion symmetry. Instead, the enhancement in SHG originates mainly from the localization of the electric field at the wavelengths of both the fundamental light and the second harmonic.

### 3.3 SHG enhancement factors calculated for the MoS<sub>2</sub> layers on the SiO<sub>2</sub>/Si and Au/SiO<sub>2</sub> substrates

As mentioned above, the localization of the electric field at the wavelengths of both the fundamental light and the second harmonic may significantly enhance the SHG. We employed the FDTD technique to simulate the electric field distributions in the MoS<sub>2</sub> layers at both wavelengths and derive the enhancement factor for SHG according to the formula given as follows:<sup>43–45</sup>

$$I_{\text{SHG}} \propto f^4(\omega)f^2(2\omega)I_{\text{in}}^2, \quad (1)$$

where  $I_{\text{SHG}}$  and  $I_{\text{in}}$  are the intensities of SHG and incident light,  $f(\omega)$  and  $f(2\omega)$  denote the electric field enhancement factors at the frequencies of the fundamental light and the second harmonic, respectively.

The electric field intensity distributions in the MoS<sub>2</sub> layers with  $d = 1\text{L}$  and  $d = 17$  nm on the SiO<sub>2</sub>/Si substrate are calculated for the fundamental light at 800 nm and the second harmonic at 400 nm, as shown in Fig. 3(A) and (B). At 800 nm, the enhancement factors for the electric field intensity (*i.e.*  $(E/E_0)^2$ ) are found to be similar for  $d = 1\text{L}$  and  $d = 17$  nm. At 400 nm, however, the enhancement factor for  $d = 1\text{L}$  ( $\sim 2.31$ ) is much larger than that for  $d = 17$  nm ( $\sim 0.14$ ). Therefore, the enhancement factor in SHG for  $d = 1\text{L}$  is expected to be much larger than that for  $d = 17$  nm without considering the inversion symmetry. In Fig. 3(C) and (D), we present the electric field intensity distributions for the MoS<sub>2</sub> layers with the same thickness on the Au/SiO<sub>2</sub> substrate for comparison. It is noticed that the enhancement factor for the electric field intensity at 800 nm achieved in the 17 nm-thick MoS<sub>2</sub> layer increased significantly from 2.81 to 37.69 when the substrate is changed from SiO<sub>2</sub>/Si to Au/SiO<sub>2</sub>. In comparison, the enhancement factor achieved in the single-layer MoS<sub>2</sub> remains nearly unchanged. Consequently, the enhancement factor in SHG achieved in the 17 nm-thick MoS<sub>2</sub> layer is about 25 times that achieved in the single-layer MoS<sub>2</sub>. In Fig. 4(A), we show the dependence of the SHG intensity on the thickness of the MoS<sub>2</sub> layer on the two types of substrates derived by using eqn (1). A monotonic reduction in the SHG enhancement factor is found for the MoS<sub>2</sub> layers on the SiO<sub>2</sub>/Si substrate. In contrast, the maximum enhancement factor in SHG is observed at a thickness of  $d = 17$  nm for the MoS<sub>2</sub> layers on the Au/SiO<sub>2</sub> substrate. For the MoS<sub>2</sub> layers with thickness smaller and larger than this optimum value, a rapid decrease of the SHG enhancement factor is seen. Another remarkable feature shown in Fig. 4(A) is the maximum enhancement factor achieved in the 17 nm-thick MoS<sub>2</sub> layer on the Au/SiO<sub>2</sub> substrate, which is about 16

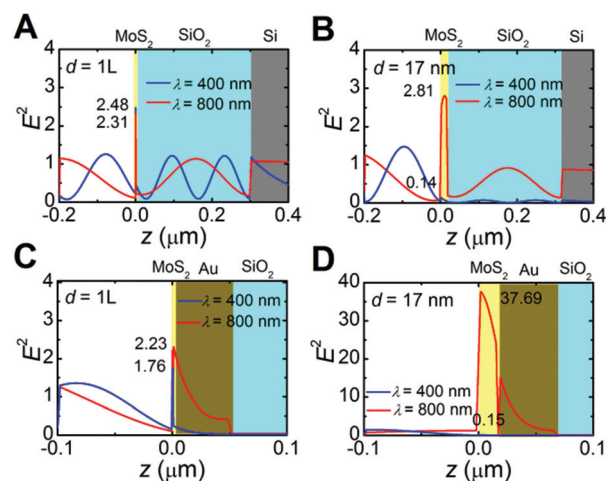


**Fig. 3** Electric field intensity distributions in the MoS<sub>2</sub> layers with  $d = 1\text{L}$  (A) and  $d = 17$  nm (B) on the SiO<sub>2</sub>/Si substrate. (C) and (D) show the electric field intensity distributions in the MoS<sub>2</sub> layers with  $d = 1\text{L}$  and  $d = 17$  nm on the Au/SiO<sub>2</sub> substrate, respectively. In each case, the enhancement factors for the electric field intensity at both the fundamental light and the second harmonic are provided.

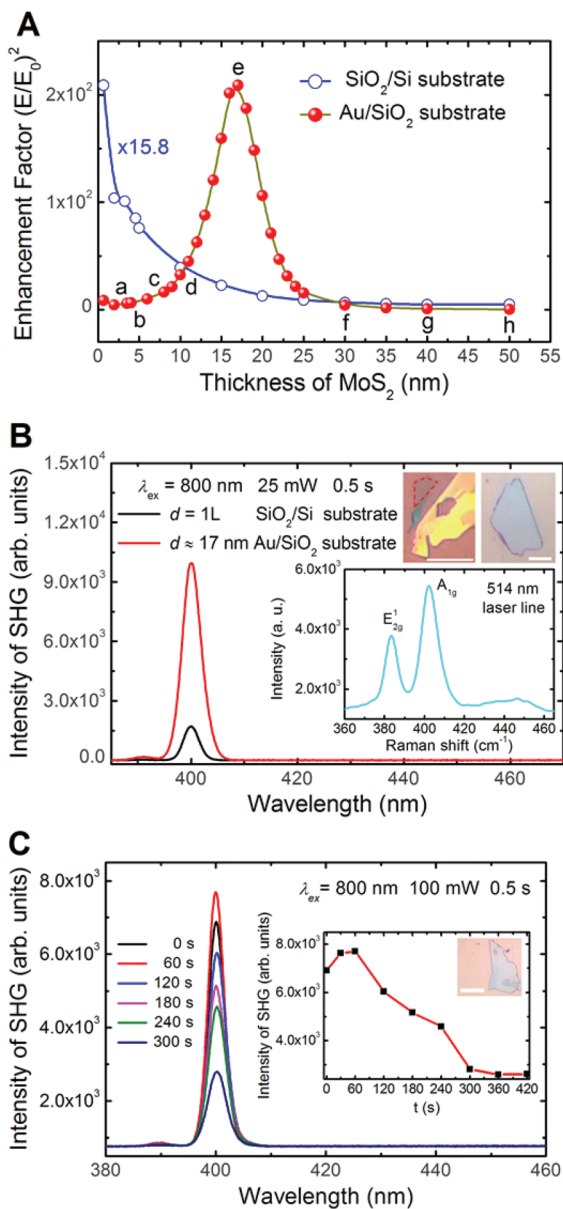


**Fig. 4** (A) Dependence of the SHG enhancement factor on the thickness of the MoS<sub>2</sub> layer on the SiO<sub>2</sub>/Si and Au/SiO<sub>2</sub> substrates. (B) Non-linear response spectra of the single-layer MoS<sub>2</sub> on the SiO<sub>2</sub>/Si substrate and the 17 nm-thick MoS<sub>2</sub> layer on the Au/SiO<sub>2</sub> substrate. The insets show the images of the MoS<sub>2</sub> layers on the SiO<sub>2</sub>/Si and Au/SiO<sub>2</sub> substrates where the single-layer MoS<sub>2</sub> is indicated by the dashed curve. The length of the scale bar is 10  $\mu$ m. The Raman spectrum for the single-layer MoS<sub>2</sub> on the SiO<sub>2</sub>/Si substrate is also provided as an inset. (C) Evolution of the nonlinear response spectrum of a MoS<sub>2</sub> layer on the Au/SiO<sub>2</sub> substrate irradiated with 100 mW fs laser light with increasing irradiation time. The inset shows the dependence of the SHG intensity on the irradiation time. The image of the sample is also provided and the length of the scale bar is 10  $\mu$ m.

times larger than that obtained in the single-layer MoS<sub>2</sub> on the SiO<sub>2</sub>/Si substrate. This explains why the SHG becomes dominated by the localization of the electric field in the MoS<sub>2</sub> layers on the Au/SiO<sub>2</sub> substrate.

In order to confirm the enhancement of SHG achieved in the MoS<sub>2</sub> layers on the Au/SiO<sub>2</sub> substrate, we compared the intensity of SHG for the single-layer MoS<sub>2</sub> on the SiO<sub>2</sub>/Si substrate with that for the 17 nm-thick MoS<sub>2</sub> layer on the Au/SiO<sub>2</sub> substrate, as shown in Fig. 4(B). The single-layer MoS<sub>2</sub> was verified by the frequency difference between the E<sub>2g</sub><sup>1</sup> and A<sub>1g</sub> modes in the Raman spectrum which was measured to be  $\sim 18.8$  cm<sup>-1</sup> (see the inset of Fig. 4(B)). It can be seen that the intensity of SHG for the 17 nm-thick MoS<sub>2</sub> layer is about 5.8 times larger than that for the single-layer MoS<sub>2</sub>. However, this value is smaller than that estimated by using eqn (1) which is 15.8. Previously, it was found that MoS<sub>2</sub> with odd layers on a SiO<sub>2</sub>/Si substrate exhibited much stronger SHG as compared to MoS<sub>2</sub> with even layers where the inversion symmetry leads to the cancellation of SHG.<sup>30–34</sup> For the MoS<sub>2</sub> layers on the Au/SiO<sub>2</sub> substrate, the inversion symmetry is broken due to the existence of the gold film and the SHG becomes dominated by the localization of the electric field. In this case, we did not find a significant difference in the intensity of SHG for MoS<sub>2</sub> with odd and even layers, as evidenced in the ablation process of the thick MoS<sub>2</sub> layers described later. Since the effect of symmetry has not been completely removed, an accurate prediction of the enhancement factor for SHG cannot be obtained by using eqn (1) in which only the enhancement of the electric field is taken into account. In addition, the distribution of electric field intensity in the 17 nm thick MoS<sub>2</sub> layer is not uniform, as can be seen in Fig. 3(D). The enhancement factor for SHG was overestimated because we chose the maximum electric field intensity to calculate the enhancement factor for SHG. All these reasons are responsible for the discrepancy observed between the theoretical prediction and the experimental observation when we compared the intensity of SHG for the single-layer MoS<sub>2</sub> on the SiO<sub>2</sub>/Si substrate and the 17 nm-thick MoS<sub>2</sub> layer on the Au/SiO<sub>2</sub> substrate. Anyway, a completely different dependence of the SHG enhancement factor on the thickness is expected for the MoS<sub>2</sub> layers on the Au/SiO<sub>2</sub> substrate.

In Fig. 4(C), we present an experimental result verifying the calculated thickness dependence of SHG intensity for the MoS<sub>2</sub> layers on the Au/SiO<sub>2</sub> substrate. It shows the evolution of the nonlinear response spectrum of a MoS<sub>2</sub> layer with increasing irradiation time when a fs laser light of 100 mW was focused on it. The peak intensity of the SHG as a function of irradiation time is shown in the inset. The MoS<sub>2</sub> layer was ablated by the fs laser light after absorbing sufficiently large energy and its thickness was reduced with increasing irradiation time. It is noticed that an increase in the SHG intensity appeared immediately at  $t = 0$  s. For  $t > 60$  s, a decrease of the SHG intensity was observed with increasing irradiation time. This phenomenon clearly indicates that there exists an optimum thickness at which the strongest SHG can be achieved. Before the ablation, the color of the MoS<sub>2</sub> layer is light blue and its initial thickness is larger than 17 nm. After the ablation, the thickness is reduced to smaller than 17 nm and the color changes to deep sky blue (see also ESI Fig. S7 and S8†).

### 3.4. Optical data storage demonstrated by using the MoS<sub>2</sub> layers on the Au/SiO<sub>2</sub> substrate

The modification of the thickness dependence of SHG induced by the Au/SiO<sub>2</sub> substrate offers us the opportunity to realize optical data storage by engineering the SHG intensity through thinning the MoS<sub>2</sub> layer. Supposing that we have a MoS<sub>2</sub> layer with very strong SHG ( $\sim 17$  nm), its thickness can be reduced by laser ablation. Apart from SHG, another non-linear optical process occurring during the excitation of the MoS<sub>2</sub> layer by using a fs laser light is two-photon absorption (TPA). Although bulk MoS<sub>2</sub> does not exhibit efficient two-photon-induced luminescence because of the indirect bandgap, the relaxation of the hot electrons created by TPA will lead to a significant temperature rise of the MoS<sub>2</sub> layer. An ablation of the MoS<sub>2</sub> layer will occur once the excitation intensity of the fs laser is sufficiently large, exceeding the ablation threshold of the MoS<sub>2</sub> layer. Since the TPA is also proportional to the enhancement in the electric field intensity, the ablation threshold for the MoS<sub>2</sub> layers is expected to depend strongly on their thicknesses. The lowest threshold is expected for the MoS<sub>2</sub> layer with  $d = 17$  nm. Once the thickness of the MoS<sub>2</sub> layer is reduced, the SHG intensity is reduced accordingly. This behavior can be exploited to realize optical data storage.

In experiments, we chose a MoS<sub>2</sub> layer with  $d \sim 17$  nm which is expected to have strong SHG. The correlation between the color of the MoS<sub>2</sub> layer and its thickness will help us to make this choice. For optical data storage, a letter "T" was recorded in the MoS<sub>2</sub> layer by using a recording power of

50 mW and an irradiation time of 20 ms. The pixel size was chosen to be  $0.20 \times 0.20 \mu\text{m}^2$ . After that, a scanning of SHG signal was performed on the MoS<sub>2</sub> layer by using a readout power of 3 mW and an integration time of 50 ms. The image obtained by scanning the SHG signal over the MoS<sub>2</sub> layer is shown in Fig. 5(D). It can be seen that the letter "T" recorded in the MoS<sub>2</sub> layer was successfully extracted, indicating that the MoS<sub>2</sub> layer on the Au/SiO<sub>2</sub> substrate can be employed for optical data storage. In Fig. 5(A) and (B), we also show the microscopy images for the MoS<sub>2</sub> layer before and after the optical data storage. A letter "T" is clearly seen in Fig. 5(B) because of the change in color from light blue to deep sky blue. It means that one can illuminate the MoS<sub>2</sub> layer with a white light to realize a fast data readout if the change in thickness is large. In the case when the change in thickness is small, the data can only be read out by detecting the SHG intensity.

## 4 Conclusions

In summary, we have investigated the linear and nonlinear optical responses of the MoS<sub>2</sub> layers on the Au/SiO<sub>2</sub> substrate and found significant modifications as compared to those on the SiO<sub>2</sub>/Si substrate. Apart from the change in color, it was found that the dependence of SHG on the thickness of the MoS<sub>2</sub> layers is also modified and the strongest SHG appears in the MoS<sub>2</sub> layer with a thickness of  $\sim 17$  nm. It was revealed by the FDTD simulation that the localization of the electric field in the MoS<sub>2</sub> layers leads to a significant enhancement in SHG which governs the dependence of the SHG on the thickness of the MoS<sub>2</sub> layers. The modified dependence of SHG on the thickness allows us to realize optical data storage which was demonstrated in a MoS<sub>2</sub> layer with a thickness of  $\sim 17$  nm on the Au/SiO<sub>2</sub> substrate. This finding paves the way for using appropriate substrates to engineer the linear and nonlinear optical properties of MoS<sub>2</sub> layers for various practical applications.

## Acknowledgements

The authors acknowledge the financial support from the National Natural Science Foundation of China (Grant No. 51171066 and 11374109) and the Ministry of Education (Grant No. 20114407110002).

## Notes and references

- 1 K. S. Novoselov, A. K. Geim, D. Jiang, Y. Zhang, S. V. Dubonos, I. V. Grigorieva and A. A. Firsov, *Science*, 2004, **306**, 666–669.
- 2 K. S. Novoselov, D. Jiang, F. Schedin, T. J. Booth, V. V. Khotkevich, S. V. Morozov and A. K. Geim, *Proc. Natl. Acad. Sci. U. S. A.*, 2005, **102**, 10451.
- 3 K. S. Novoselov, *Rev. Mod. Phys.*, 2011, **83**, 837–849.

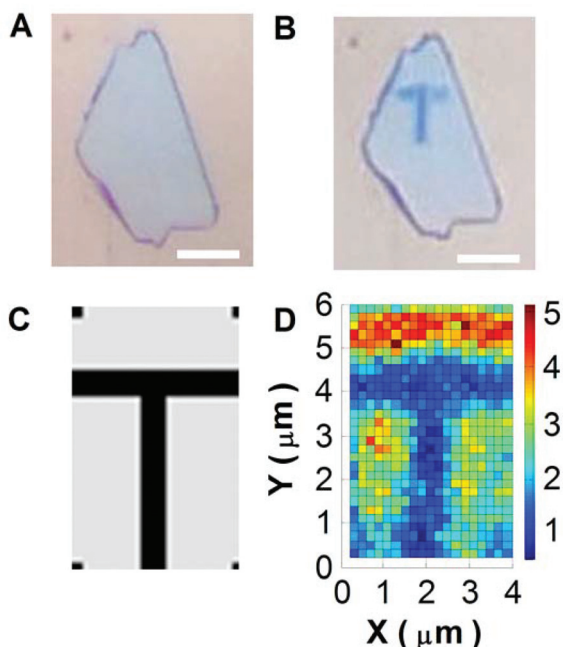


Fig. 5 Microscope images for the MoS<sub>2</sub> sheet before (A) and after (B) optical data storage (recording a letter "T"). The length of the scale bar is 5  $\mu\text{m}$ . (C) and (D) are the original pattern of letter "T" and the pattern extracted by reading the SHG intensity of the MoS<sub>2</sub> sheet.

- 4 J. N. Coleman, M. Lotya, A. O'Neill, S. D. Bergin, P. J. King, U. Khan, K. Young, A. Gaucher, S. De, R. J. Smith, I. V. Shvets, S. K. Arora, G. Stanton, H. Y. Kim, K. Lee, G. T. Kim, G. S. Duesberg, T. Hallam, J. J. Boland, J. J. Wang, J. F. Donegan, J. C. Grunlan, G. Moriarty, A. Shmeliov, R. J. Nicholls, J. M. Perkins, E. M. Grievson, K. Theuwissen, D. W. McComb, P. D. Nellist and V. Nicolosi, *Science*, 2011, **331**, 568–571.
- 5 K. S. Novoselov and A. H. Castro Neto, *Phys. Scr.*, 2012, **T146**, 014006.
- 6 Q. H. Wang, K. Kalantar-Zadeh, A. Kis, J. N. Coleman and M. S. Strano, *Nat. Nanotechnol.*, 2012, **7**, 699–712.
- 7 H. Zeng, G. Liu, J. Dai, Y. Yan, B. Zhu, R. He, L. Xie, S. Xu, X. Chen, W. Yao and X. Cui, *Sci. Rep.*, 2013, **3**, 1608.
- 8 Z. Gong, G. Liu, H. Yu, D. Xiao, X. Cui, X. Xu and W. Yao, *Nat. Commun.*, 2013, **4**, 2053.
- 9 M. Xu, T. Liang, M. Shi and H. Chen, *Chem. Rev.*, 2013, **113**, 3766–3798.
- 10 K. F. Mak, C. Lee, J. Hone, J. Shan and T. F. Heinz, *Phys. Rev. Lett.*, 2010, **105**, 136805.
- 11 A. Splendiani, L. Sun, Y. Zhang, T. Li, J. Kim, C. Y. Chim, G. Galli and F. Wang, *Nano Lett.*, 2010, **10**, 1271–1275.
- 12 K. F. Mak, K. He, J. Shan and T. F. Heinz, *Nat. Nanotechnol.*, 2012, **7**, 494–498.
- 13 H. Zeng, J. Dai, W. Yao, D. Xiao and X. Cui, *Nat. Nanotechnol.*, 2012, **7**, 490–493.
- 14 T. Cao, G. Wang, W. Han, H. Ye, C. Zhu, J. Shi, Q. Niu, P. Tan, E. Wang, B. Liu and J. Feng, *Nat. Commun.*, 2012, **3**, 887.
- 15 S. Tongay, J. Zhou, C. Ataca, K. Lo, T. S. Matthews, J. Li, J. C. Grossman and J. Wu, *Nano Lett.*, 2012, **12**, 5576–5580.
- 16 R. Ganatra and Q. Zhang, *ACS Nano*, 2014, **8**, 4074–4099.
- 17 H. Zhu, Y. Wang, J. Xiao, M. Liu, S. Xiong, Z. J. Wong, Z. Ye, Y. Ye, X. Yin and X. Zhang, *Nat. Nanotechnol.*, 2015, **10**, 151–155.
- 18 Y. Lin, X. Ling, L. Yu, S. Huang, A. L. Hsu, Y.-H. Lee, J. Kong, M. S. Dresselhaus and T. Palacios, *Nano Lett.*, 2014, **14**, 5569–5576.
- 19 L. Liu, S. B. Kumar, Y. Ouyang and J. Guo, *IEEE Trans. Electron Devices*, 2011, **58**, 3042–3047.
- 20 Y. Yoon, K. Ganapathi and S. Salahuddin, *Nano Lett.*, 2011, **11**, 3768–3773.
- 21 H. Wang, L. L. Yu, Y. H. Lee, Y. M. Shi, A. Hsu, M. L. Chin, L. J. Li, M. Dubey, J. Kong and T. Palacios, *Nano Lett.*, 2012, **12**, 4674–4680.
- 22 B. Radisavljevic, M. B. Whitwick and A. Kis, *ACS Nano*, 2011, **5**, 9934–9938.
- 23 S. Bertolazzi, J. Brivio and A. Kis, *ACS Nano*, 2011, **5**, 9703–9709.
- 24 Q. Y. He, Z. Y. Zeng, Z. Y. Yin, H. Li, S. X. Wu, X. Huang and H. Zhang, *Small*, 2012, **8**, 2994–2999.
- 25 J. Pu, Y. Yomogida, K. K. Liu, L. J. Li, Y. Iwasa and T. Takenobu, *Nano Lett.*, 2012, **12**, 4013–4017.
- 26 Z. Yin, H. Li, H. Li, L. Jiang, Y. Shi, Y. Sun, G. Lu, Q. Zhang, X. Chen and H. Zhang, *ACS Nano*, 2012, **6**, 74–80.
- 27 H. S. Lee, S. W. Min, Y. G. Chang, M. K. Park, T. Nam, H. Kim, J. H. Kim, S. Ryu and S. Im, *Nano Lett.*, 2012, **12**, 3695–3700.
- 28 M. Shanmugam, T. Bansal, C. A. Durcan and B. Yu, *Appl. Phys. Lett.*, 2012, **100**, 153901.
- 29 R. W. Boyd, *Nonlinear Optics*, 3rd edn, Academic, San Diego, 2008.
- 30 N. Kumar, S. Najmaei, Q. Cui, F. Ceballos, P. M. Ajayan, J. Lou and H. Zhao, *Phys. Rev. B: Condens. Matter*, 2013, **87**, 161403(R).
- 31 L. M. Malard, T. V. Alencar, A. P. M. Barboza, K. F. Mak and A. M. dePaula, *Phys. Rev. B: Condens. Matter*, 2013, **87**, 201401(R).
- 32 Y. Li, Y. Rao, K. F. Mak, Y. You, S. Wang, C. R. Dean and T. F. Heinz, *Nano Lett.*, 2013, **13**, 3329–3333.
- 33 W. T. Hsu, Z. A. Zhao, L. J. Li, C. H. Chen, M. H. Chiu, P. S. Chang, Y. C. Chou and W. H. Chang, *ACS Nano*, 2014, **8**, 2951–2958.
- 34 X. B. Yin, Z. L. Ye, D. A. Chenet, Y. Ye, K. O'Brien, J. C. Hone and X. Zhang, *Science*, 2014, **344**, 488–490.
- 35 R. Wang, H. C. Chien, J. Kumar, N. Kumar, H. Y. Chiu and H. Zhao, *Appl. Mater. Interfaces*, 2014, **6**, 314–318.
- 36 K. S. Yee, *IEEE Trans. Antennas Propag.*, 1966, **14**, 302–307. In this paper, a commercially available software developed by the Rsoft Design Group (<http://www.rsoftdesign.com>) is used for the numerical simulations.
- 37 C. C. Shen, Y. T. Hsu, L. J. Li and H. L. Liu, *Appl. Phys. Express*, 2013, **6**, 125801.
- 38 R. A. Neville and B. L. Evans, *Phys. Status Solidi B*, 1976, **73**, 597–606.
- 39 H. Li, Q. Zhang, C. C. R. Yap, B. K. Tay, T. H. T. Edwin, A. Olivier and D. Baillargeat, *Adv. Funct. Mater.*, 2012, **22**, 1385–1390.
- 40 M. A. Kats, R. Blanchard, P. Genevet and F. Capasso, *Nat. Mater.*, 2013, **12**, 20–24.
- 41 M. A. Kats, S. J. Byrnes, R. Blanchard, M. Kolle, P. Genevet, J. Aizenberg and F. Capasso, *Appl. Phys. Lett.*, 2013, **103**, 101104.
- 42 M. A. Kats, R. Blanchard, S. Ramanathan and F. Capasso, *Opt. Photonics News*, 2014, **25**, 40–47.
- 43 A. Wokaun, in *Solid State Physics*, ed. H. Ehrenreich, T. Thurnbull and F. Seitz, Academic, New York, 1984, vol. 38, p. 223.
- 44 C. Hubert, L. Billot, P. M. Adam, R. Bachelot, P. Royer, J. Grand, D. Gindre, K. D. Dorkenoo and A. Ford, *Appl. Phys. Lett.*, 2007, **90**, 181105.
- 45 C. Li, C. Zhang, Z. Huang, X. Li, Q. Dai, S. Lan and S. Tie, *J. Phys. Chem. C*, 2013, **117**, 24625–24631.